Formation of Fluorescent Metal (Au, Ag) Nanoclusters Capped in Bovine Serum Albumin Followed by Fluorescence and Spectroscopy

ARTICLE *in* THE JOURNAL OF PHYSICAL CHEMISTRY C · MAY 2011

Impact Factor: 4.77 · DOI: 10.1021/jp111820b

6 AUTHORS, INCLUDING:

Xavier Le Guével
University Grenoble-Alpes
28 PUBLICATIONS **462** CITATIONS
SEE PROFILE

Klaus Hollemeyer
Universität des Saarlandes
39 PUBLICATIONS **532** CITATIONS
SEE PROFILE

Marc Schneider
Universität des Saarlandes
110 PUBLICATIONS **1,982** CITATIONS
SEE PROFILE

THE JOURNAL OF PHYSICAL CHEMISTRY C

ARTICLE

pubs.acs.org/JPCC

Formation of Fluorescent Metal (Au, Ag) Nanoclusters Capped in Bovine Serum Albumin Followed by Fluorescence and Spectroscopy

Xavier Le Guével,[†] Benjamin Hötzer,[‡] Gregor Jung,[‡] Klaus Hollemeyer,[§] Vanessa Trouillet,[⊥] and Marc Schneider*[,†]

[†]Pharmaceutical Nanotechnology, [‡]Department of Biophysical Chemistry, and [§]Biochemical Engineering Institute, Saarland University, Saarbrücken, Germany

[⊥]Institute for Materials Research III, KIT-Campus North, P.O. Box 3640, 76021 Karlsruhe, Germany

Supporting Information

ABSTRACT:

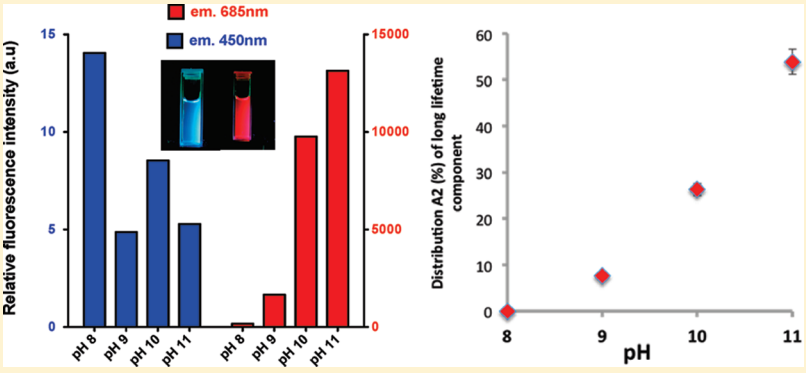

Fluorescent noble metal (Au, Ag) nanoclusters have been biolabeled to bovine serum albumin (BSA) by wet chemistry. Spectroscopic and fluorescence investigations relate the role of the pH and the nature of the reducing agent to the size and the oxidation state of metal clusters. Blue-emitting (λ = 450 nm) small gold nanoclusters (eight atoms) prepared at pH 8 weakly bonded to BSA grow at higher pH to form red-emitting (λ = 690 nm) bigger clusters (25 atoms) covalently bonded to BSA via the sulfur group. X-ray photoelectron spectroscopy (XPS) measurements indicate the presence of Au(I) only for the big clusters. Small silver nanoclusters labeled to the protein with a fluorescence emission in the red region are synthesized in the presence of a strong reducing agent and present only Ag(0). Steady-state and lifetime measurements confirm the crucial impact of the size and the oxidation state of Au(I) on the stabilization of the metal core inside the protein and on the presence of a long lifetime component (τ > 170 ns).

1. INTRODUCTION

Fluorescent metal (gold, silver) nanoclusters (NCs) have stimulated extensive interest in the past decade because of their remarkable optical properties for a wide range of applications such as sensing,[1−4] biolabeling,[5−7] and imaging.[8,9] Gold and silver NCs have sizes comparable to the Fermi wavelength of an electron (i.e., the electron de Broglie wavelength at the Fermi level: ∼0.5 nm for Au and Ag) and exhibit molecular-like behavior including discrete electronic states and size-dependent fluorescence. Much effort has been made in the last 20 years to understand the structural and electronic properties of metal nanoclusters through a combination of theory and experiments.[10,11] The Jellium $E_{Fermi}/N_{1/3}$ energy scaling law was used as a model to describe the size-dependent electronic structure and relative electronic transitions of the small clusters.[12] Since then, many groups have confirmed the presence of NCs with a magic number of atoms (n = 8, 11, 13, 18, 22, 25, 28, 39, 55, ...) using several templates such as dendrimers,[13−15] DNA,[5,6] proteins,[2,9,16,17] polymers,[18,19] and polyelectrolytes.[20] Recently, a new route was developed to synthesize gold nanoclusters protected with glutathione by etching.[21−23] It allows for the creation of NCs with a discrete and intense fluorescence emission from the blue to the infrared. Structural and electronic properties of these clusters depend strongly on the nature of the ligand and of the metal−ligand interaction to the fluorescence enhancement.[24] However, only a few studies have been reported on the growth of metal clusters labeled to bovine serum albumin (BSA) and, in particular, to the relation between the structure of the nanoclusters in the protein and their fluorescence properties.

We describe in this article the growing process and the nature of the interaction of metal−protein using gold and silver NCs capped in BSA. Structural investigation and fluorescence

Received: December 13, 2010
Revised: April 26, 2011
Published: May 13, 2011

Table 1. Synthesis Condition of Metal (Au, Ag) Nanoclusters Labeled to Bovine Serum Albumin (BSA)

	Au_8−BSA	Au_{25}−BSA	Ag_8−BSA
molar ratio metal/protein	33	33	16.5
reducing agent	ascorbic acid	ascorbic acid	sodium borohydride
pH	8	11	7
temperature	37 °C	37 °C	0 °C
reaction time	5 h	5 h	4 h (in the dark)

properties highlight the impact of the pH and the nature of the reducing agent to the oxidation state of the metal, the geometry of the protein, and the electronic charge transfer.

2. EXPERIMENTAL: MATERIALS AND METHODS

2.1. Preparation of Metal (Au, Ag) Nanoclusters. All chemicals have been purchased from Sigma-Aldrich (Germany) and have been used without any further purification. Ultrapure water (18.2 MΩ) was used in all experiments.

Synthesis of Gold Nanoclusters (Au−BSA). Small gold clusters (n = 8) with a blue fluorescence emission were prepared by adding 5 mL aqueous solution of $HAuCl_4$ (10 mM) to 5 mL of bovine serum albumin (BSA 96%; 20 mg/mL in water) under vigorous stirring at 37 °C. Fifty microliters of ascorbic acid (0.35 mg/mL) was added dropwise to trigger the formation of gold nanoclusters without using a large amount of BSA. The reaction proceeded for 5 h at 37 °C while the pH was maintained at 8. The solution called Au_8−BSA had a pale yellow color. Big gold clusters Au_{25}−BSA (n = 25) with a red fluorescence emission were prepared in the same way at a higher pH of 11 with the addition of NaOH (1 M).[16,17] The solution turned from pale yellow to a dark orange solution after 3 h indicating the formation of big clusters. Two more hours were necessary to complete the reduction of BSA-encapsulated Au precursor and to increase the yield of big nanoclusters. A series of Au−BSA solutions were prepared at different pH levels ranging from 8 to 11 to determine the impact of the pH on the gold nanocluster growth.

Synthesis of Silver Nanoclusters (Ag−BSA). Briefly, a 5 mL aqueous solution of $AgNO_3$ (5 mM) was reacted with 5 mL of bovine serum albumin (BSA 96%; 20 mg/mL) in the dark at 0 °C under vigorous stirring. After 5 min, 20 μL of a freshly prepared aqueous solution of $NaBH_4$ (5 mM) was introduced to quickly reduce the Ag^+ ions. The reaction was allowed to continue for another 4 h. The solution Ag_8−BSA with a red fluorescence emission changed from colorless to pale brown after a few minutes. Because of the high sensitivity of silver ions, it is crucial to control parameters such as light exposure and temperature in order to obtain a high concentration of silver nanoclusters.[25]

All the samples were kept refrigerated and did not show any precipitation after three months. Experimental conditions to prepare gold and silver nanoclusters are collected in Table 1.

2.2. Instrumentation. Matrix-assisted laser desorption ionization time-of-flight mass spectrometry (MALDI-TOF MS) (Applied Biosystems 4800 Maldi Tof/Tof) measurements of Au−BSA and Ag−BSA were performed using α-cyano-4-hydroxycinnamic acid (CHCA) as a matrix. Spectra were collected in the positive mode. The samples were freeze-dried and were characterized by infrared spectroscopy between 4000 and 400 cm^{-1} with a resolution of 4 cm^{-1} on a Tensor 24 Fourier transform infrared (FTIR) spectrometer from Bruker. X-ray photoelectron spectroscopy (XPS) investigation was performed in a K-alpha spectrometer (ThermoFisher Scientific, East Grinstead, United Kingdom) using a microfocused, monochromated Al Kα X-ray source (200 μm spot size). The K-alpha charge compensation system was employed during analysis using electrons of 8 eV energy and low-energy argon ions to prevent any localized charge buildup. The kinetic energy of the electrons was measured by a 180° hemispherical energy analyzer operated in the constant analyzer energy mode (CAE) at 50 eV pass energy for elemental spectra. Data acquisition and processing using the Thermo Avantage software is described elsewhere.[26] All spectra were referenced to the C 1s peak at 285.0 eV binding energy (C−H) and were controlled by means of the well-known photoelectron peaks of Cu, Ag, and Au. UV−visible extinction spectra of gold and silver nanoclusters were measured using a Lambda 35 scan UV−visible spectrophotometer (Perkin-Elmer) in transmission mode. Fluorescence scans of the samples were performed on a Tecan infinite M200 instrument using microplates. Lifetime values were measured by time-correlated single-photon counting under magic-angle conditions. The excitation source was a pulsed diode laser (LDH-P-C-405, Picoquant, Germany) emitting at 405 nm. The laser was driven by an oscillator module (PDL 808-MC Sepia, Picoquant, Germany) at a repetition rate of 2.5 MHz. Fluorescence was detected in 90° geometry after spectral filtering (HQ 685-70, AHF Analysentechnik, Germany) by an avalanche photodiode (PDM 100ct SPAD, Micron Photon Devices, Italy). Electronic signals were recorded by a stand-alone TCSPC module (PicoHarp300, Picoquant, Germany), and the readout was synchronized by software (SymPhoTime, Picoquant, Germany). The instrument response function (IRF) was recorded under described conditions by replacing the sample with a Ludox solution (Sigma-Aldrich, Germany). The full width at half-maximum (FWHM) was about 300 ps. Analysis of the data was done by the software FluoFit (Picoquant, Germany). For all measurements, $\chi^2 < 1.2$ could be obtained by deconvolution fitting according to a biexponential decay.

3. RESULTS AND DISCUSSION

3.1. Nanoclusters-Protein Spectroscopic Investigation. *3.1.1. Gold Nanoclusters.* Oxidation state and binding properties of gold nanoclusters labeled to BSA were determined by XPS. Au $4f_{7/2}$ for Au_{25}−BSA (Figure 1a) could be deconvoluted into two distinct components centered at 84.1 and 85.2 eV assigned to Au(0) and Au(I), respectively.[22] These results are consistent with XPS measurements performed by Xie et al.[17] where approximately the same amount of Au(I) in BSA (∼10%) was observed. The presence of Au(I) could be considered as intermediate species located on the core surface of the clusters.[27] Au(I) species are partially reduced to valence (0) during the reaction stabilizing the nanoclusters because of the reduction by the tyrosine residue at high pH and by the presence of ascorbic acid. Authors correlate this reduction to the hybridization of the empty 6s/6p orbital and the filled $5d^{10}$ orbital.[22] The binding energies of S $2p_{3/2}$ at 161.9 and 168.1 eV (Figure 1b) are attributed to sulfur bound to gold and oxidized sulfur, respectively. The peak at 161.9 eV corresponds to a covalent interaction of gold nanoclusters[28,29] with the sulfur groups of the cysteine (35 cysteines per BSA). Moreover, an oxidation of the sulfur

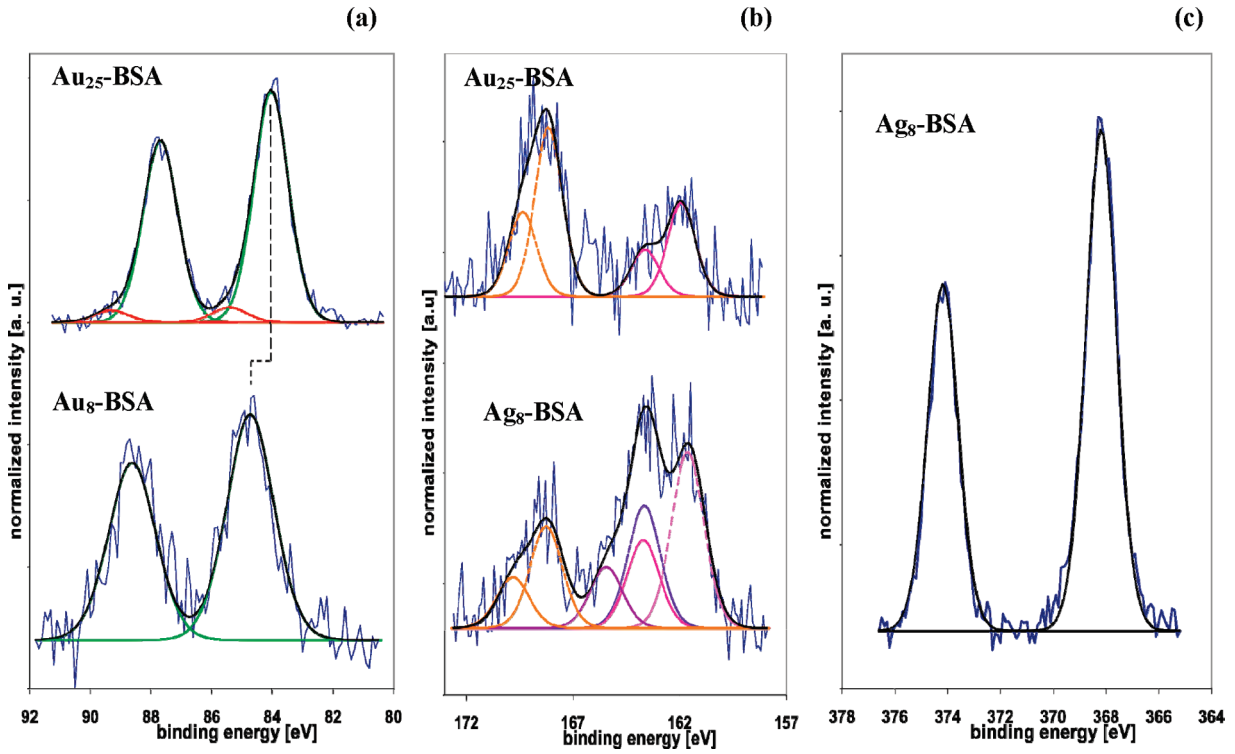

Figure 1. XPS spectra: (a) Au $4f_{7/2}$ of Au_{25}−BSA shows two peaks, one peak at 84.1 eV (green curve) and the other at 85.4 eV (red curve), which are attributed to Au(0) (90%) and Au(I) (10%), respectively. The shift to the higher binding energy of Au(0) at 84.7 eV for the small clusters Au_8−BSA is related to the reduction of the core size. (b) S $2p_{3/2}$ confirms the presence of gold bound to sulfur (pink curve) for Au_{25}−BSA and Ag_8−BSA samples with peaks at 161.9 and 161.4 eV, respectively. Unbound sulfur (purple curve) and oxidized sulfur (yellow curve) are present in both samples. (c) Ag 3d of Ag_8−BSA samples shows the core reduction of silver with a Ag $3d_{5/2}$ peak at 368.2 eV.

might be a consequence of the degradation of the protein because of the high pH (11) used during the synthesis. The Au:S (at 161.9 eV) atomic ratio has been evaluated to 1:1. However, this value has to be considered carefully because of the low concentration of gold and sulfur in the sample (∼0.3 wt %) and the detection limit of the method.

Compared to Au_{25}−BSA (Figure 1a), the small clusters Au_8−BSA present only Au(0) with a binding energy shifted to higher energy from 84.1 to 84.7 eV. This behavior was expected and was reported by other authors who demonstrated increasing binding energy of the metal clusters with decreasing cluster size related to the positive charge left on the metal clusters.[27] S 2p of small clusters presents no component related to Au−S bonds (data not shown) thus indicating a high degree of freedom of the Au_8 NCs in the protein. Another explanation for the positive chemical shift of the high binding energy for Au_8−BSA compared to Au_{25}−BSA could be also related to the high concentration of gold ions (Au(I), partially reduced at pH 8 in the presence of a weak reducing agent, stabilized in the protein by the carboxyl groups of the Trp residues[30] and by the phenolic groups of the Tyr residues[17]). However, we noticed the absence of (a) XPS peaks related to Au−S and (b) contribution of Au(I) component after deconvolution of Au $4f_{7/2}$. Those observations also make the hypothesis of the core reduction quite consistent.

MALDI-TOF measurement is a common technique used to determine the nature of the core and the ligand for metal thiolate nanoclusters M-SR.[11] Figure 2a shows that the MALDI MS spectrum of Au_{25}−BSA sample is composed of several intense peaks between 2000 and 12 000 m/z with spacing of m/z 197 and 229 corresponding to the loss of Au and Au−S, respectively. The peak-expanded view in the same figure illustrates the additional spacing of m/z 32 between each triplet because of the sulfur. A Gaussian distribution of the peaks is clearly visible in the spectra and indicates a high polydispersity in nanocluster size in the protein. We assume that the features are assignable to Au_nS^{m+} and that the maximum intensity is related to the presence of a high population of 22−25 gold atoms by considering spectroscopic measurements made by other authors on the same material.[16,23,31] Desorption-ionization is a highly complex physicochemical process not completely understood yet especially if noncovalent bound complexes are involved. A gas-phase fragmentation of Au clusters may be able to alter the true sizes of the original clusters. Even if a second analysis method is desirable to detect the cluster sizes independently, Hamouda et al. demonstrated recently a recorded gas spectrum similar to the one obtained in solution using Au_{25} NCs capped in glutathione.[32] The small clusters Au_8−BSA did not show any characteristic peaks of gold clusters. This result is in agreement with XPS data which could be explained by the weak binding of these clusters in BSA that prevents the detection of Au NCs by ionization.

Infrared spectroscopy (FTIR) is one of the most common methods of characterizing protein conformational change and the analysis of the secondary structure in particular.[33] The protein amide I in the region 1600−1700 cm^{-1} (mainly CO stretch) and the amide II band ≈1548 cm^{-1} (C−N stretch coupled with N−H bending mode) are related to the secondary structure of the protein. The amide I band is more sensitive to the change of protein secondary structure than amide II because of

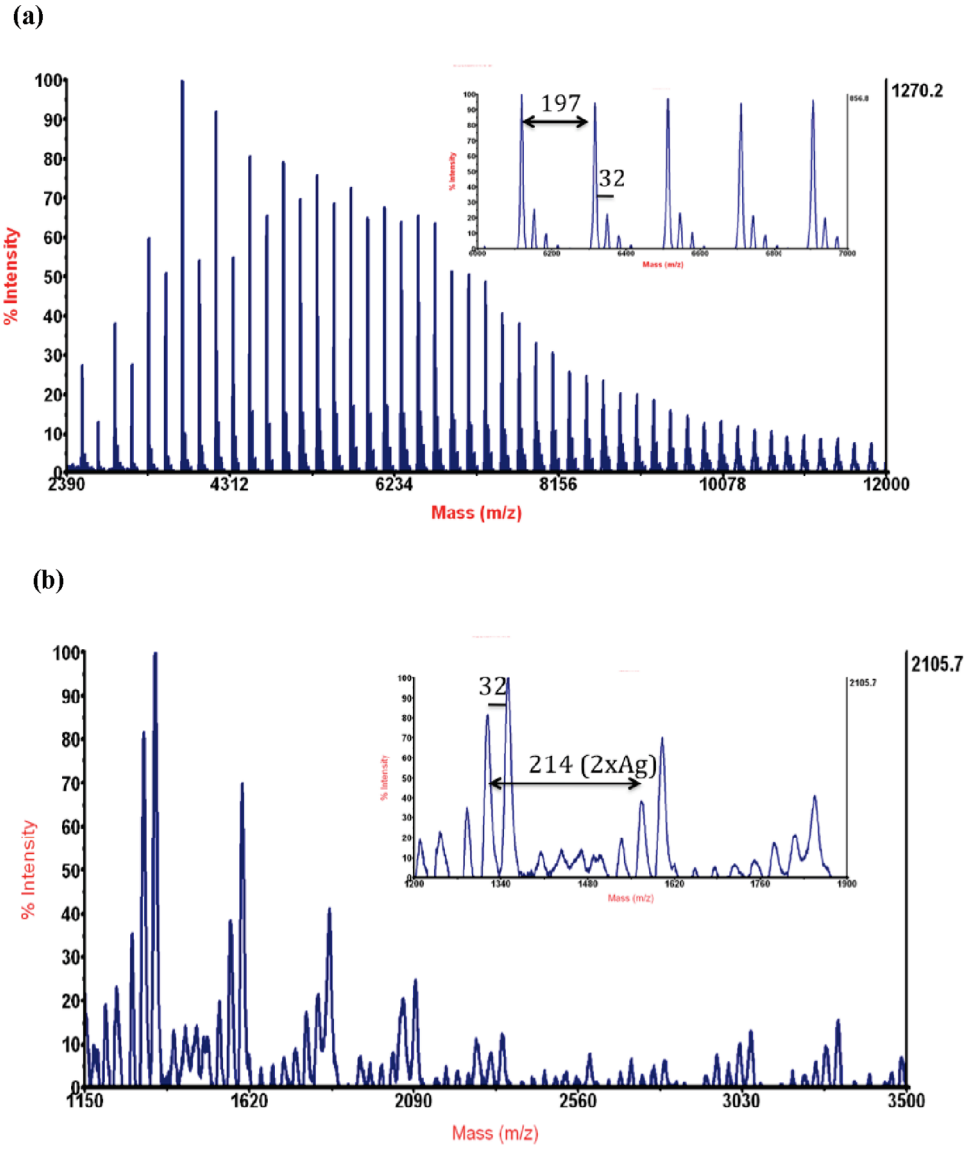

Figure 2. MALDI-TOF MS of (a) Au_{25}—BSA and (b) Ag_8—BSA recorded in the positive mode. Au_{25}—BSA shows a Gaussian distribution of peaks separated by m/z 197 and 32 (expanded view) corresponding to gold and sulfur. The maximum intensity is related to the presence of 22—25 gold atoms. Ag_8—BSA presents a series of triplets separated by the spacing m/z 107 or 214 corresponding to one and two silver atoms and each triplet by the spacing 32 for sulfur (expanded view). It corresponds to a distribution of Ag_nS^{m+} nanoclusters with $8 \geq n \geq 2$ and $0 \geq m \geq 3$.

transition dipole coupling. Moreover, the broad band assigned to amide I has been fully investigated by many authors and can provide information about different types of secondary structures such as α-helix (1648—1657 cm^{-1}), β-sheets (1623—1641 cm^{-1}), turns (1662—1657 cm^{-1}), and disordered (1642—1657 cm^{-1}).[33] Figure 3 presents the infrared spectra of BSA, Au_{25}—BSA, and Au_8—BSA in the range 1700—1350 cm^{-1}. The characteristic vibration peaks of BSA are present after gold nanocluster labeling. The inset in Figure 3 shows an obvious shift of the amide I band to lower wavenumbers after conjugation from 1650 cm^{-1} to 1640—1634 cm^{-1}. This trend indicates a modification of the secondary structure of the BSA after labeling. Furthermore, a decrease in the intensity of the peak at higher wavenumber indicates that fewer helical structures are present. To prove that the change of the protein geometry cannot be attributed only to the pH condition, free BSA and gold-labeled BSA prepared at pH 8 and 11 were measured (see Figure S1 of the Supporting Information). The results indicate a significant contribution of gold NCs to the shift of amide I to the lower wavenumber. An increase of pH leads to an increase of the peak intensity centered at 1515 cm^{-1} which could correspond to a deprotonation of Tyr-OH.[34] Moreover, the band located at 1400—1450 cm^{-1} assigned to the vibration of tryptophan (Trp) becomes drastically larger when nanoclusters are prepared at high pH for the Au_{25}—BSA sample. Thus, for Au_8—BSA which is synthesized at pH 8, this effect is less pronounced. This result is in agreement with XPS measurements which showed a high oxidation degree of the sulfur for gold nanoclusters prepared in basic conditions.

3.1.2. Silver Nanoclusters. The XPS spectrum of Ag_8—BSA is illustrated in Figure 1c and shows a Ag $3d_{5/2}$ peak centered at 368.2 eV which corresponds to Ag(0). The absence of Ag(I) might be related in this case to the use of sodium borohydride which reduces completely silver ions in BSA. The S $2p_{3/2}$ peak can be deconvoluted into three different components at 161.4,

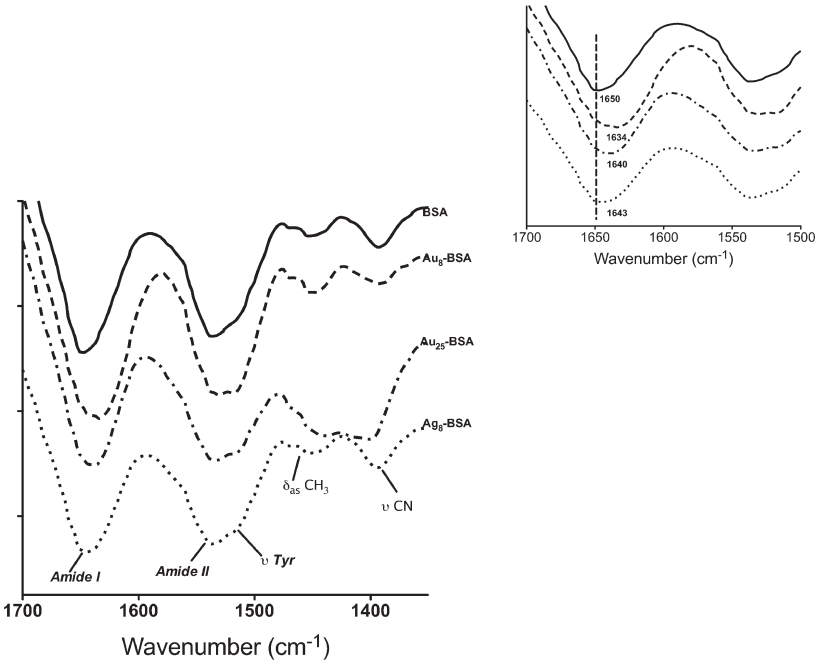

Figure 3. FTIR spectra of BSA, Au_8—BSA, Au_{25}—BSA, and Ag_8—BSA freeze-dried samples. The inset illustrates the shift of the amide I peak at 1650 cm^{-1} to the lower wavenumber corresponding to the labeling of metal clusters to BSA.

Table 2. Photophysical Properties of Au—BSA and Ag—BSA Samples

	$\lambda_{exc.}$ (nm)	$\lambda_{em.}$ (nm)	τ_1 (ns)[a]	A_1 (%)	τ_2 (ns)[a]	A_2 (%)	ϕ (%)[b]
Au_8—BSA	370	450	0.8 ± 0.2	92.4	3.0 ± 0.3	7.6	6.07
Au_{25}—BSA	370; 530	685	1.78 ± 0.3	46.1	184 ± 7	53.9	5.53
Ag_8—BSA	490	685	1 ± 0.2	84	5.3 ± 0.3	16	1.46

[a] $\lambda_{exc.}$ = 405 nm; emission filter 440-40 for Au_8—BSA and 685-70 for Au_{25}—BSA and Ag_8—BSA. Lifetime values were evaluated with a biexponential fit. [b] Quantum yield determined from the equation $QY = (I_s \times QY_r)/I_r$ where I_s is the integrated emission intensity of the sample; QY_r and I_r are the quantum yield and integrated emission intensity of the reference sample, respectively. Quinine sulfate (QY = 0.53 in 0.5 M sulfuric acid) was chosen as a reference for Au_8—BSA sample; Rhodamine 6G (QY = 0.95 in ethanol) was chosen for Au_{25}—BSA and Ag_8—BSA samples. Samples were diluted with deionized water for spectral measurements to yield an absorbance ~0.1 at 360 nm for Au_8—BSA and at 480 nm for Au_{25}—BSA and Ag—BSA samples.

163.6, and 168.0 eV which are attributed to Ag—S, S, and oxidized sulfur, respectively. The presence of a peak assigned to unbound sulfur and the low contribution of the oxidized sulfur suggest that the silver nanoclusters are only partially bound to the sulfur groups and that a neutral pH during the growing process does not involve a strong oxidation of the sulfur atom. The atomic ratio between Ag and bound S (at 161.4 eV) is about 1:1 with an atomic concentration of silver around 0.15%.

Patterns of MALDI peaks depicted in Figure 2b show the presence of a series of three peaks with m/z spacing of 107 or 214 between each series and 32 between isolated peaks in the triplets for the lowest m/z ions (1000—4000). This spacing is attributed to the presence of silver atoms bonded to m sulfur atoms and indicates the presence of two to eight silver atoms bonded to multiple thiol groups $Ag_{2-8}S_m$ in the protein BSA. The intensity of the triplets decreased for higher m/z values and proved the absence of big Ag NCs in the protein. The infrared spectrum of the silver clusters shows the same trend as the gold clusters in BSA with a shift of the amide I band to the lower wavenumber after labeling (Figure 3).

Silver nanoclusters are covalently bonded to BSA via sulfur groups and are completely reduced to Ag(0). They present a population of small clusters between two and eight atoms. BSA exhibits a modification of its secondary structure after gold and silver labeling. Spectroscopic study of gold nanoclusters trapped in the protein BSA indicated a covalent binding interaction between the metal and the sulfur groups of the thiol-bearing cysteine residues of BSA for the big clusters and a weak interaction with the protein for the small clusters. Au NCs prepared at high pH show a polydisperse population of mainly 25 atoms with two oxidation states Au(0) and Au(I). Only Au(0) is present at pH 8.

3.2. Optical Properties Related to Cluster Size. Fluorescence wavelengths, lifetime, and quantum yield of the metal nanoclusters are collected in Table 2.

3.2.1. Silver Nanoclusters. Growth of stable silver NCs in BSA with high yield proves to be difficult to control probably because of the sensitivity of Ag^+ ions and the use of BH_4^- ions, a relatively harsh reductant. Figure 4a shows the absorbance curves of Ag_8—BSA 30 min and 4 h after addition of sodium borohydride. The shoulder of the peak located at 430 nm slowly disappears with the emergence of a rather weak broad band at 520 nm thus giving the solution a pale brown color. The presence of these absorbance peaks have been assigned by other authors to

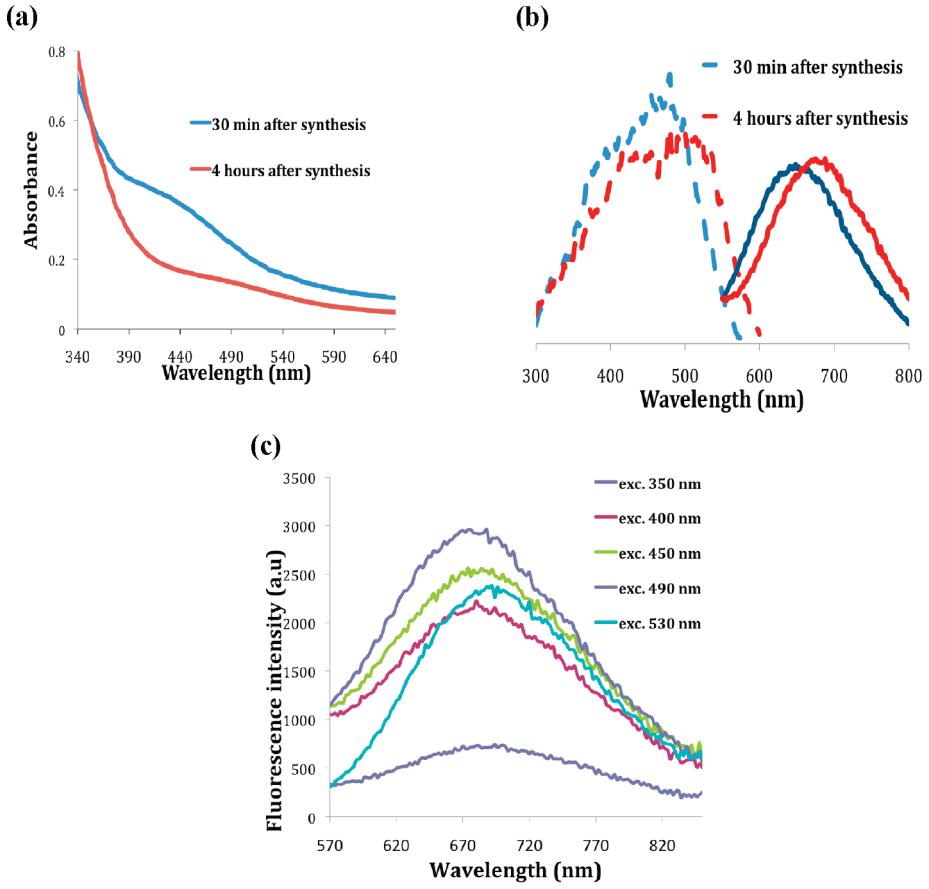

Figure 4. Absorbance spectra (a) of Ag_8—BSA show a decrease of a band centered at 440 nm with an emergence of a broad band at 520 nm with the aging time related to the formation of silver nanoclusters. (b) Excitation/emission scans of Ag_8—BSA are shifted to the longer wavelength between 30 min (in blue) and 4 h (in red) because of the growth of the silver clusters. (c) Shift of the emission wavelength under different excitation wavelengths (nm) indicates the fluorescence stability of the clusters.

the reduction of silver nanoclusters Ag_n^+ where n varied from 2 to 8.[6,15,35,36] Moreover, the shift to the higher absorbance wavelength during the growth of Ag NCs is accompanied by a 30 nm red-shift in the excitation/emission wavelengths (Figure 4b) indicating an increased cluster size. Red luminescence of Ag—BSA was observed upon excitation at 500 nm. Maximum excitation and emission peaks are located at 490/690 nm with no shift or decreased intensity after 1 month in refrigerated storage. Rao and Pradeep[36] found the same fluorescence properties for Ag_7 and Ag_8 silver nanoclusters produced by etching. Even if no dramatic shift in fluorescence emission is observed for a wide range of excitation wavelengths (350—530 nm) (see Figure 4c), the emission bandwidth remains broad pointing out the necessity to improve the monodispersity of the cluster atomic number in the protein. Indeed, the presence of NCs with different excitation/emission properties through the visible range generates the interband transitions (sp←d).[10,37] Quantum yield (QY) of Ag—BSA is relatively low with an estimated value of 1.46% (Rhodamine 6G; 0.95 in ethanol used as reference). This low QY might be related to the low concentration of Ag NCs in BSA proved by XPS with the presence of free sulfur of cysteine not bound to silver and by infrared spectroscopy indicating only a small modification of the protein conformation. Lifetime measurements of Ag—BSA present a biexponential fluorescence decay: τ_1 = 1.0 ns (84%) and τ_2 = 5.3 ns (16%).

3.2.2. Gold Nanoclusters. Growth of gold clusters in BSA as a function of the pH has been followed by steady-state fluorescence and lifetime measurements. Excitation and emission spectra of Au_8—BSA prepared at pH 8 and Au_{25}—BSA prepared at pH 11 are plotted in Figure 5a. It is known that BSA fluoresces with a blue emission under UV irradiation. Fluorescence measurement of BSA with and without small gold clusters (see Figure S2 of the Supporting Information) in the presence of ascorbic acid demonstrates the intrinsic fluorescence properties of Au_8 where the blue emission of Au_8—BSA is mainly related to the abundance of the fluorescent small gold nanoclusters and not to the autofluorescence of the protein BSA. The Au_8—BSA sample presents a blue emission with a maximum intensity at $\lambda_{em.}$ = 450 nm and a single excitation band centered at 370 nm. Small clusters are first formed in the protein because the growth of Au_8 clusters results from the extraordinary stability of this magic cluster with closed electronic shells.[12,38] However, the monodispersity of the cluster remains difficult to control in a wet chemistry synthesis, and the asymmetric fluorescence emission spectra of Au_8—BSA confirm the presence of bigger clusters (Figure S2 of the Supporting Information). Au_{25}—BSA emit in the red region ($\lambda_{em.}$ = 685 nm) with a high Stokes shift (>150 nm) and have two excitation peaks located at 370 and 530 nm. Theoretically, photophysical properties of Au_{25} clusters should present discrete excitation—emission bands related to highest occupied molecular orbital—lowest unoccupied molecular orbital

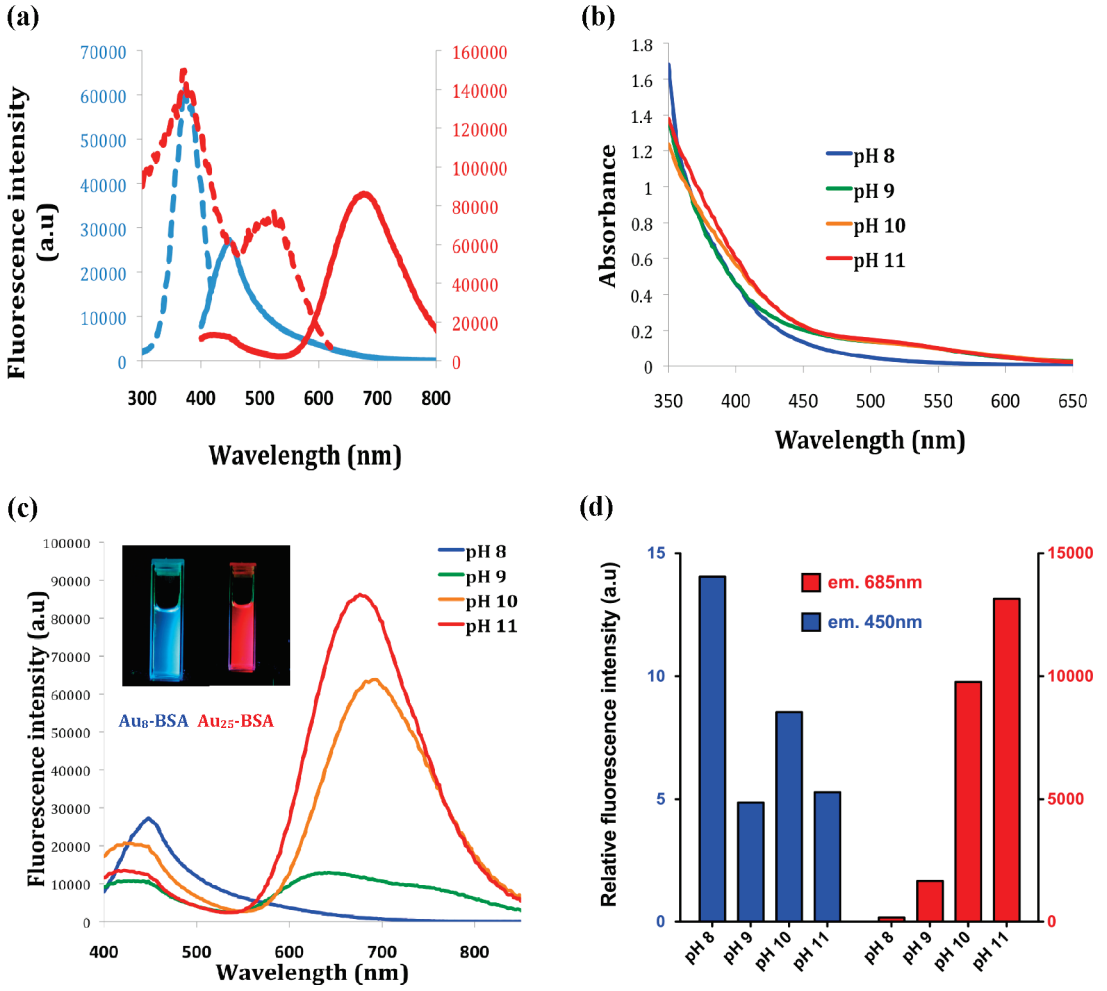

Figure 5. (a) Excitation/emission scans of Au_8—BSA (in blue) and Au_{25}—BSA (in red) measured at their maximum intensities. (b) Absorbance spectra and (c) emission scans ($\lambda_{exc.}$= 360 nm) of Au—BSA samples prepared at different pHs. (d) Relative fluorescence intensity of Au—BSA at $\lambda_{em.}$ = 450 and 685 nm under UV irradiation ($\lambda_{exc.}$= 360 nm) with gain = 100.

(HOMO—LUMO) electronic transitions at 530—700 nm.[7,21] The two excitation and emission peaks for Au_{25}—BSA underline the presence of a polydisperse distribution of gold clusters with different sizes in addition to the broad emission spectrum. Absorbance spectra plotted in Figure 5b show only a weak broad band at 520 nm for samples prepared at high pH. This plasmon band could be attributed to the presence of a few gold nanoparticles bigger than 3 nm but also to the electronic transition between the ligand and the metal core. Both samples do not present any significant shift of their fluorescence emission upon excitation in the range 350—550 nm confirming the stability of these nanoclusters in the protein (data not shown). Fluorescence measurements on Au—BSA samples prepared at different pH levels from 8 to 11 are collected in Figure 5c. As reported in a previous paper for Au NCs protected in dendrimers,[39] raising the pH produces an increase in red fluorescence emission and a slight decrease in blue emission related to the small clusters. Figure 5d shows the enhancement of the relative fluorescence intensity in the red region with the increase of the pH thus indicating the growth of bigger gold clusters in BSA. The fluorescence of the small clusters dropped at higher pH compared to the preparation at pH 8. We assume that this trend is related to (1) the consumption of the small clusters during the growing process and to (2) the energy transfer from the small clusters to the bigger ones under UV excitation. QYs of Au_8—BSA and Au_{25}—BSA were determined by a comparative method using quinine sulfate (QY = 0.54 in 0.05 M sulfuric acid) and Rhodamine 6G (0.95 in ethanol), respectively, as references. Values are in the range of 5—7% (see Table 2) which are consistent with measurements performed on gold nanoclusters in different templates with the same size and the same fluorescence emission.[9,31,40]

Lifetime measurements of Au—BSA samples were performed at two different emission wavelengths: $\lambda_{em.}$ = 440 nm corresponding to the small clusters Au_8—BSA and $\lambda_{em.}$ = 670 nm corresponding to the big clusters Au_{25}—BSA. All data were fitted by global biexponential fitting and are gathered in Table 3. Increased pH during the synthesis led to increased amounts of big clusters in solution and therefore to an intense red fluorescent emission. Lifetime values of the blue-emitting clusters seem to be independent of the pH and the growth of the big clusters with τ_1 = 0.7 ns (~20%) and τ_2 = 5.0 ns (~80%). Considering the energy level spacing to be too small within the sp bands to give a visible emission, these emission lifetimes are assumed to be mainly attributed to singlet transitions between low-lying d bands and excited sp bands of gold nanoclusters.[38] More interesting is the presence of a very long lifetime component

Table 3. Lifetime Measurements of Au−BSA Prepared at Different pHs (8−11) Using Two Filters: 440-40 nm and 685-70 nm with an Excitation Wavelength at 405 nm[a]

	emission filter 440-40 nm				emission filter 685-70 nm			
Au−BSA	τ1 (ns)	A1(%)	τ2 (ns)	A2(%)	τ1 (ns)	A1(%)	τ2 (ns)	A2(%)
pH 8	{0.7 ± 0.1}	21	{5.0 ± 0.2}	79	0.8 ± 0.2	100	{184 ± 10}	0
pH 9		17		83	1.78 ± 0.2	92.4		7.6
pH 10		29		71	1.78 ± 0.2	73.7		26.3
pH 11		23		77	1.78 ± 0.2	46.1		53.9

[a] For all measurements, $\chi^2 < 1.2$ could be obtained by deconvolution fitting according to a biexponential decay. A_n (%) corresponds to the lifetime distribution for each component.

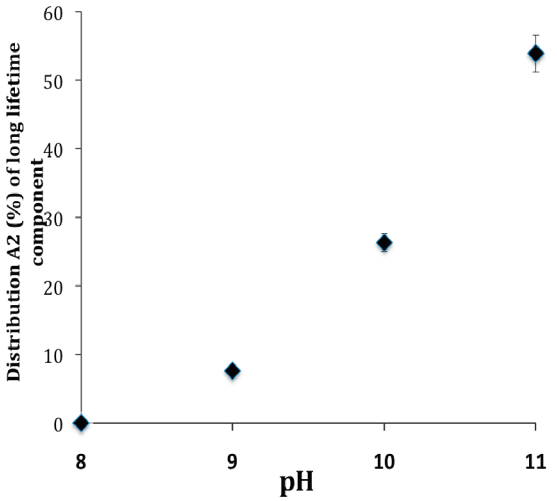

Figure 6. Evolution of the distribution of the long lifetime component τ = 184 ns as a function of pH used to prepare Au−BSA. There is a clear relation between the pH used during the synthesis and the enhancement of the long lifetime distribution related to the concentration of big clusters.

(τ = 184 ns) in the red wavelength range when big clusters appear during the synthesis. Moreover, the distribution of this long component increases with the pH indicating the correlation between the concentration of the big clusters and the long lifetime component (Figure 6). Zheng et al. considered the presence of this long lifetime component to be due to a triplet−singlet intraband transition.[12] Another explanation for the origin of this lifetime could be related to the oxidation state of the gold inside the BSA. It is known that Au(I) species tend to aggregate by strong aurophilic interactions because of hybridization of the empty 6s/6p orbital and filled 5d orbital.[41] Then, thiol−Au(I) complexes can display ligand−metal charge transfer and metal(I)−metal(I) interactions. Indeed, XPS investigation confirms the presence of Au(I) (∼10%) only for the big clusters Au_{25}−BSA and the absence of Au(I) for the small clusters Au_8−BSA which present no long lifetime component. Furthermore, silver nanoclusters with the oxidation state Ag(0) emit in the red region (600−750 nm) with no long lifetime component as well. Recently, Wu and Jin determined the ligand's role in the fluorescence of nanoclusters and demonstrated the importance of the oxidation state of the metal and the energy transfer from the ligand to the metal to enhance the fluorescence.[24] Even if silver and gold have slightly different electronic properties, the data suggest that (1) the long lifetime component is related to the size of the clusters and to the oxidation state of the metal and (2) the distribution of the long lifetime increases with the concentration of big clusters in the template (protein). However, further work needs to be done to fully understand the mechanism of charge transfer of gold and silver nanoclusters, triplet and singlet excited states, as a function of their oxidation state.

In summary, the growth of big size Au NCs (25 atoms) with red emission is pH induced from small eight atom clusters which have a blue emission. The long lifetime detected only for Au_{25}−BSA is attributed to metal−metal and metal−ligand charge transfer and to the oxidation state of the metal. Small silver and gold nanoclusters present similar fluorescent properties which differ mainly by a different energy gap.

CONCLUSION

Silver and gold nanoclusters with a red emission ($\lambda_{em.}$ = 685 nm) have been synthesized by wet chemistry in bovine serum albumin (BSA). We show in this paper the importance of the nature of the reducing agent and pH on the oxidation state of the clusters, the geometry of the protein, and the growth of the clusters. Structural investigation indicated that small (≤8 atoms) metal (gold and silver) nanoclusters grow at pH 7−8 with a weak interaction with the protein. Raising the pH to 11 for gold clusters promotes the formation of the big clusters with a polydisperse distribution of mainly 25 gold atoms covalently bound to BSA via sulfur groups. Metal clusters involved a modification of the protein backbone after labeling with a decrease of the helical structures and an oxidation of the sulfur groups at high pH. Fluorescence study confirmed the two-step formation of 22−25 gold atoms in BSA with the growth of blue-emitting small clusters followed by an aggregation of polydisperse red-emitting big clusters and an energy transfer between small and large clusters. Moreover, XPS and fluorescence measurements confirm the importance of the oxidation state to the stability of the metal nanoclusters in the protein and to the presence of a long fluorescence lifetime component (τ > 170 ns) being connected with the large clusters.

ASSOCIATED CONTENT

Supporting Information. There is additional material available such as infrared spectra of freeze-dried samples (Figure S1) and emission and excitation spectra of Au_8−BSA considering autofluorescence of BSA (Figure S2). This information is available free of charge via the Internet at http://pubs.acs.org.

■ ACKNOWLEDGMENT

Xavier Le Guével thanks the Andalusian Regional Ministry of Health the Andalusian Initiative for Advanced Therapies — Fundacion Progreso y Salud for supporting the research activity and the German Research Foundation (DFG, Grant JU-650/2-2).

■ REFERENCES

(1) Shiang, Y. C.; Huang, C. C.; Chang, H. T. *Chem. Commun.* **2009**, 3437.
(2) Wei, H.; Wang, Z. D.; Yang, L. M.; Tian, S. L.; Hou, C. J.; Lu, Y. *Analyst* **2010**, *135*, 1406.
(3) Shang, L.; Dong, S. J. *Biosens. Bioelectron.* **2009**, *24*, 1569.
(4) Huang, C. C.; Chen, C. T.; Shiang, Y. C.; Lin, Z. H.; Chang, H. T. *Anal. Chem.* **2009**, *81*, 875.
(5) Richards, C. I.; Choi, S.; Hsiang, J. C.; Antoku, Y.; Vosch, T.; Bongiorno, A.; Tzeng, Y. L.; Dickson, R. M. *J. Am. Chem. Soc.* **2008**, *130*, 5038.
(6) Yu, J. H.; Choi, S.; Dickson, R. M. *Angew. Chem., Int. Ed.* **2009**, *48*, 318.
(7) Lin, C. A. J.; Yang, T. Y.; Lee, C. H.; Huang, S. H.; Sperling, R. A.; Zanella, M.; Li, J. K.; Shen, J. L.; Wang, H. H.; Yeh, H. I.; Parak, W. J.; Chang, W. H. *ACS Nano* **2009**, *3*, 395.
(8) Yu, J.; Patel, S. A.; Dickson, R. M. *Angew. Chem., Int. Ed.* **2007**, *46*, 2028.
(9) Retnakumari, A.; Setua, S.; Menon, D.; Ravindran, P.; Muhammed, H.; Pradeep, T.; Nair, S.; Koyakutty, M. *Nanotechnology* **2010**, 21.
(10) Zhu, M.; Aikens, C. M.; Hollander, F. J.; Schatz, G. C.; Jin, R. *J. Am. Chem. Soc.* **2008**, *130*, 5883.
(11) Schaaff, T. G. *Anal. Chem.* **2004**, *76*, 6187.
(12) Zheng, J.; Nicovich, P. R.; Dickson, R. M. *Annu. Rev. Phys. Chem.* **2007**, *58*, 409.
(13) Lesniak, W. G.; Kariapper, M. S. T.; Nair, B. M.; Tan, W.; Hutson, A.; Balogh, L. P.; Khan, M. K. *Bioconjugate Chem.* **2007**, *18*, 1148.
(14) Shi, X. Y.; Ganser, T. R.; Sun, K.; Balogh, L. P.; Baker, J. R. *Nanotechnology* **2006**, *17*, 1072.
(15) Zheng, J.; Dickson, R. M. *J. Am. Chem. Soc.* **2002**, *124*, 13982.
(16) Simms, G. A.; Padmos, J. D.; Zhang, P. *J. Chem. Phys.* **2009**, 131.
(17) Xie, J. P.; Zheng, Y. G.; Ying, J. Y. *J. Am. Chem. Soc.* **2009**, *131*, 888.
(18) Duan, H. W.; Nie, S. M. *J. Am. Chem. Soc.* **2007**, *129*, 2412.
(19) Zhang, J. G.; Xu, S. Q.; Kumacheva, E. *Adv. Mater.* **2005**, *17*, 2336.
(20) Shang, L.; Dong, S. J. *Chem. Commun.* **2008**, 1088.
(21) Muhammed, M. A. H.; Ramesh, S.; Sinha, S. S.; Pal, S. K.; Pradeep, T. *Nano Res.* **2008**, *1*, 333.
(22) Negishi, Y.; Nobusada, K.; Tsukuda, T. *J. Am. Chem. Soc.* **2005**, *127*, 5261.
(23) Shibu, E. S.; Muhammed, M. A. H.; Tsukuda, T.; Pradeep, T. *J. Phys. Chem. C* **2008**, *112*, 12168.
(24) Wu, Z. K.; Jin, R. C. *Nano Lett.* **2010**, *10*, 2568.
(25) Shen, Z.; Duan, H. W.; Frey, H. *Adv. Mater.* **2007**, *19*, 349.
(26) Parry, K. L.; Shard, A. G.; Short, R. D.; White, R. G.; Whittle, J. D.; Wright, A. *Surf. Interface Anal.* **2006**, *38*, 1497.
(27) Tanaka, A.; Takeda, Y.; Imamura, M.; Sato, S. *Phys. Rev. B* **2003**, 68.
(28) Kummer, K.; Vyalikh, D. V.; Gavrila, G.; Kade, A.; Weigel-Jech, M.; Mertig, M.; Molodtsov, S. L. *J. Electron Spectrosc. Relat. Phenom.* **2008**, *163*, 59.
(29) Cavalleri, O.; Oliveri, L.; Dacca, A.; Parodi, R.; Rolandi, R. *Appl. Surf. Sci.* **2001**, *175*, 357.
(30) Antoine, R.; Bertorelle, F.; Broyer, M.; Compagnon, I.; Dugourd, P.; Kulesza, A.; Mitric, R.; Bonacic-Koutecky, V. *Angew. Chem., Int. Ed.* **2009**, *48*, 7829.
(31) Muhammed, M. A. H.; Verma, P. K.; Pal, S. K.; Kumar, R. C. A.; Paul, S.; Omkumar, R. V.; Pradeep, T. *Chem.—Eur. J.* **2009**, *15*, 10110.
(32) Hamouda, R.; Bellina, B.; Bertorelle, F.; Compagnon, I.; Antoine, R.; Broyer, M.; Rayane, D.; Dugourd, P. *J. Phys. Chem. Lett.* **2010**, *1*, 3189.
(33) Barth, A. *Biochim. Biophys. Acta, Bioenerg.* **2007**, *1767*, 1073.
(34) Shang, L.; Wang, Y. Z.; Jiang, J. G.; Dong, S. J. *Langmuir* **2007**, *23*, 2714.
(35) Diez, I.; Pusa, M.; Kulmala, S.; Jiang, H.; Walther, A.; Goldmann, A. S.; Muller, A. H. E.; Ikkala, O.; Ras, R. H. A. *Angew. Chem., Int. Ed.* **2009**, *48*, 2122.
(36) Rao, T. U. B.; Pradeep, T. *Angew. Chem., Int. Ed.* **2010**, *49*, 3925.
(37) Gagliardi, L.; Pyykko, P. *Angew. Chem., Int. Ed.* **2004**, *43*, 1573.
(38) Zheng, J.; Petty, J. T.; Dickson, R. M. *J. Am. Chem. Soc.* **2003**, *125*, 7780.
(39) Bao, Y. P.; Zhong, C.; Vu, D. M.; Temirov, J. P.; Dyer, R. B.; Martinez, J. S. *J. Phys. Chem. C* **2007**, *111*, 12194.
(40) Yuan, C. T.; Chou, W. C.; Tang, J.; Lin, C. A.; Chang, W. H.; Shen, J. L.; Chuu, D. S. *Opt. Express* **2009**, *17*, 16111.
(41) Pyykko, P. *Nat. Nanotechnol.* **2007**, *2*, 273.